THE ASTROPHYSICAL JOURNAL, 451:498–509, 1995 October 1

ACCRETION DISK WINDS FROM ACTIVE GALACTIC NUCLEI

N. MURRAY[1], J. CHIANG[1], S. A. GROSSMAN[1,2], AND G. M. VOIT[3]
Received 1995 February 23; accepted 1995 April 13

ABSTRACT

We present a dynamical model in which the broad absorption lines seen in some quasar spectra form in a smooth nonspherical wind from an accretion disk. On the inner edge of this wind, at $r \approx 10^{16}$ cm for a 10^8 $M_\odot$ black hole, entrained dense gas blocks soft X-rays but transmits ultraviolet photons; this allows radiation pressure on resonance lines to accelerate the outflow to $\sim 0.1c$. The wind is driven up out of the disk by a combination of radiation pressure and gas pressure. The wind is nearly in the plane of the disk, with an opening angle of $\sim 5°$. If the quasar is viewed through the wind, broad blueshifted absorption lines are seen, particularly in the resonance transitions of C IV, O VI, Ne VIII, and Lyman-α. In objects showing such blueshifted absorption, strong, soft X-ray absorption will also be seen. The wind produces emission lines at most viewing angles, which contributes significantly to the formation of the broad emission lines that characterize active galactic nuclei.

We describe self-consistent dynamical and photoionization calculations of the line radiation force on the gas. These demonstrate that the soft X-ray blocking gas modifies the spectral energy distribution of the central source so that the line driving is effective for extremely high ionization parameters. This modified spectrum also accounts for the discrepancy with previous photoionization calculations, which indicated that both the emitting and absorbing gas had a very small filling factor.

Subject headings: accretion, accretion disks — galaxies: nuclei — quasars: absorption lines

1. INTRODUCTION

Strong, broad emission lines from the resonant ultraviolet transitions of H I, O VI, N V, C IV, and Si IV are among the most prominent features in quasar spectra (Blandford, Netzer, & Woltjer 1990; Osterbrock 1989). Even more striking, but less common, are the blueshifted broad absorption lines ($\Delta v/v \sim 0.1$) of these same ions that appear in 10%–20% of optically selected quasars, known as broad absorption line quasars or BALQSOs (Turnshek 1987; Weyman et al. 1991). Lower ionization broad absorption lines of Mg II and Al III are seen in $\sim 10\%$ of optically selected BALQSOs. Aside from the absorption lines themselves, the spectra of BALQSOs are very similar to those of ordinary quasars. Probably most radio-quiet quasars have BAL material that covers 10%–20% of the total solid angle surrounding the central source (Hamman, Korista, & Morris 1993). Radio-loud quasars form a separate 10% subset, none of which are known to show broad absorption features (Stocke et al. 1992). The fact that these blueshifted lines absorb a significant fraction of the total radiative momentum suggests that they form in a radiatively accelerated wind similar to an O-star wind. However, models relying on resonance-line pressure have had difficulty keeping the wind (Drew & Boksenberg; 1984; Vitello & Shlosman 1988) or clouds (Arav, Li, & Begelman 1994) from becoming fully ionized during acceleration to one-tenth the speed of light; but see Shlosman, Vitello, & Shaviv (1985). This paper presents a model for line-driven winds from accretion disks that circumvents this problem, provides a source for the BAL material, produces the proper amount of acceleration, and explains why the frequency of BALQSOs is $\sim 10\%$. If this model is correct, the wind also plays a significant part in the formation of the broad emission lines.

Quasars emit the bulk of their luminosity ($L \approx 10^{46}$ ergs s^{-1}) in the ultraviolet band, with a substantial fraction in a power-law X-ray tail (Osterbrock 1989; Blandford et al. 1990). The short timescale of X-ray variability indicates an X-ray source size $\sim 2 \times 10^{14}$ cm. This small size, coupled with the large luminosity, suggests the presence of a massive black hole. The "standard model" adopted here, assumes that matter accretes onto this black hole through a disk that converts mass into energy with $\sim 6\%$ efficiency (for a nonrotating hole). If the black hole accretes at near the Eddington rate, its mass must be $\sim 10^8$ $M_\odot$.

The strength of the broad C III (semiforbidden) line in quasar spectra establishes that at least some of the broad-line emitting gas has a hydrogen number density $n \lesssim 10^{9.5}$ cm^{-3}. The lack of broad [O III] forbidden lines implies $n \gg 10^5$ cm^{-3}. Photoionization models for the broad-line gas yield temperatures $\sim 20{,}000$ K. The continuum can be seen through the absorbing gas, giving a firm upper limit of $\sim 2 \times 10^{24}$ cm^{-2} for the column density. The column density of the emitting gas is not so well constrained, but photoionization calculations suggest an upper limit of order 10^{23} cm^{-2} for the column of emitting gas. The length scale of the emitting gas is thus $l \sim 10^{23}$ cm^{-2}/ 10^9 cm^{-3} $= 10^{14}$ cm.

While quasar spectra provide fairly direct density and temperature estimates, the sizes of the broad-line-emitting and absorbing regions are more difficult to ascertain. The best estimates come from observations of Seyfert galaxies, which are believed to be closely related to quasars because their spectra are so similar. The dimmer ($L \approx 10^{44}$ ergs s^{-1}) but much more numerous Seyfert galaxies appear to be low-luminosity versions of quasars. Long-term monitoring of Seyfert line and continuum fluctuations shows that high-ionization lines such as N V form at small distances from the central source, while

[1] Canadian Institute for Theoretical Astrophysics, University of Toronto, Toronto, ONT, M5S 1A7, Canada.
[2] Postal address: Department of Physics and Astronomy, Northwestern University, Evanston, II 60208.
[3] Department of Physics and Astronomy, John Hopkins University, Baltimore, MD 21218.

lower ionization lines form at larger radii (Clavel et al. 1991; Reichert et al. 1994; Korista et al. 1995). The most recent efforts, involving NGC 5548 (Korista et al. 1995) and NGC 3783 (Reichert et al. 1994), find a delay between the continuum fluctuations and the response of the N v line of 1.4 days, corresponding to a radius of 3.6×10^{15} cm in NGC 5548, and a formal lag of 0 days (NGC 3783) and 1.7 days (NGC 5548) for He II. If the emitting gas is photoionized, the size of the broad-line emission region scales as the square root of the luminosity. This suggests a size of $\sim 3 \times 10^{16}$ for a quasar broad-line emission region. Since the N v absorption feature obscures Lyα emission in many BALQSOs (Turnshek 1987), the absorbing gas cannot lie within the broad-line emitting region but can be cospatial with it or outside of it.

Models for the broad absorption lines must solve both a dynamical problem and a photoionization problem. A candidate model must explain how to produce gas with a range of velocities approaching 30,000 km s^{-1} and must also explain the observed range of ionization states. Essentially all models assume photoionization equilibrium, so that the ionization state of the gas is determined by the spectral shape of the ionizing radiation and by the ionization parameter $U = n_\gamma/n$. Here, n_γ is the number density of ionizing photons, and n is the number density of hydrogen nuclei. Ideally, a model should also explain the rate of occurrence of the broad absorption lines in radio-quiet quasars as well as the lower incidence (or lack) of broad absorption in radio-loud quasars. Below we demonstrate how line-driven winds from accretion disks can solve these dynamical and ionization problems and discuss how broad emission lines might also form in disk winds.

2. GEOMETRY AND DYNAMICS

We make the following assumptions about the central engine of an active galactic nucleus (AGN):

1. There is a disk structure orbiting a black hole, as shown schematically in Figure 1.
2. The height z of the disk may increase with radius r, but $z \ll r$ at all radii.
3. The last stable orbit in the disk is at $9 \times 10^{13}(M/10^8\ M_\odot)$ (appropriate for a nonrotating hole).
4. The X-ray source is only a few times larger than this. It is represented by the dashed circle in the figure.
5. The disk is optically thick at the radii where the wind emerges from the disk, although it might be optically thin at smaller radii.

We will show below that the wind streamlines, shown as solid lines in the figure, are helical; near the surface of the disk the motion is primarily rotational, with $v_\phi \approx 10{,}000$ km s^{-1}. The wind emerges from the disk at $r \sim 10^{16}$ cm. It accelerates rapidly in the radial direction so that in most of the volume occupied by the wind $v_r \gg v_\phi \gg -v_\theta$. The streamlines rapidly approach radial lines. The steepest such radial line is shown by dotted lines in the figure. Just inside the wind lies the dense gas that shields the wind from the central X-ray source; it is labeled "hitchhiking gas."

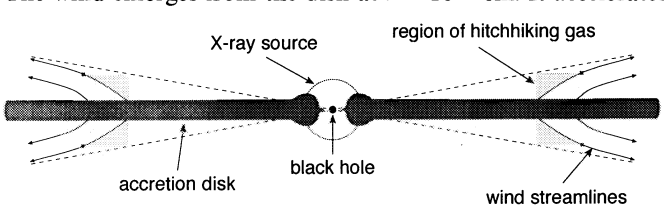

FIG. 1.—Schematic representation of a disk wind. The drawing is *not* to scale. The disk is represented by the heavily stippled region. The black circle represents the black hole. Wind streamlines are denoted by curved solid lines, which approach (*dotted*) radial lines. The critical points on the innermost streamlines are marked with crosses. The shielding gas (*lightly stippled region*) lies just inside the innermost streamline. It blocks the line of sight from the central black hole to the critical point on the innermost streamline.

In our numerical calculations we assume that the structure of the accretion disk powering the quasar follows the thin disk solution of Shakura & Sunyaev (1973), specified by the mass M of the central black hole, the mass accretion rate $\dot{M}_{\rm acc}$, the rest mass conversion efficiency η, and a viscosity parameter, which we take to be 0.1. Typically, $M = 10^8\ M_\odot$, $\dot{M}_{\rm acc} \approx 1.8\ M_\odot$ yr^{-1}, and $\eta = 0.06$. It is useful to describe the mass accretion rate in terms of Γ, equal to the luminosity L divided by the Eddington luminosity $L_{\rm edd} = 4\pi GMc/\sigma_e$, where $\sigma_e \approx 0.4$ cm^2 g^{-1}. For the above parameters, $L_{\rm edd} = 1.3 \times 10^{46}$ ergs s^{-1} and $\Gamma = 0.5$. The inner edge of the disk is at $r_1 = 6GM/c^2 \approx 9 \times 10^{13}$ cm, the outer edge of the radiation-supported part of the disk is at $\approx 3.7 \times 10^{16}$ cm, and the disk is optically thick for $r \gtrsim 9.6 r_1$. Between the last two radii the disk is flat with a half-thickness $z = z_0 \approx 1.8 \times 10^{14}(\Gamma/0.5)$ cm. From 3.7×10^{16} cm to 3.5×10^{17} cm, the height of the disk increases as $r^{21/20}$, $z = z_0(r/3.7 \times 10^{16})^{21/20}(\Gamma/0.5)^{1/5}$ cm; beyond 3.5×10^{17}, z scales as $r^{9/8}$.

There are four properties of the disk model that affect the wind. The first is the fraction of the gravitational energy that is dissipated locally in the disk and emerges as roughly thermal radiation. This fraction must be large enough to ensure that the wind is lifted sufficiently high over the disk to cover 10% of the sky as seen from the central source. Second, the disk must not flare too rapidly, or the wind will hit the disk as it flows outward. We show below that a wind streamline rises above the disk more rapidly than the radius passing through the streamline's footpoint. Thus, the disk height can increase somewhat faster than linearly with radius and still allow the wind to flow out to large distances. For example, in the Shakura-Sunyaev disk with a maximum radius of 10 pc, the opening angle of the outer disk edge is about 0.02 radians, much less than the opening angle of a disk wind. Third, we assume that the outer regions of the disk (in which the wind arises) are illuminated by the inner regions (in which the bulk of the UV flux is generated). Finally, the disk must be geometrically thin, but optically thick, at least where the wind originates.

As in the O-star wind model of Castor, Abbott, & Klein (1975, hereafter CAK), a combination of gas pressure and radiation pressure on resonance lines drives a wind from the accretion disk. The line optical depth in an accelerating wind is (Castor 1970; CAK)

$$\tau = \frac{\pi e^2}{m_e c} gf\lambda \frac{(n_l/g_l) - (n_u/g_u)}{|d(v\mu)/ds|} . \quad (1)$$

The wind speed is denoted by $v = |\boldsymbol{v}|$. The quantity s is the distance along the line between the source of the radiation and the wind, and μ is the cosine of the angle between $\boldsymbol{v}$ and that same line. The quantities n_l and n_u are the number densities of ions in the lower and upper states of the transition. The line force per gram in a wind exposed to a flux F is $g_{\rm line} = (\sigma_e F/c)\mathcal{M}(t)$, where the first factor is the acceleration due to electron scattering (Abbott 1982). The force multiplier $\mathcal{M} = kt^{-\alpha}(N_{11}/W)^\delta$ accounts for the effect of all the lines. The factor k is a constant, N_{11} is the electron number density in units of 10^{11} cm^{-3}, and W is a dilution factor. The dimensionless

optical depth t is

$$t = \frac{\sigma_e \rho v_{\rm th}}{|d(v\mu)/ds|} . \quad (2)$$

The density is denoted by ρ, and $v_{\rm th}$ is the thermal velocity. For O-star winds, Abbott finds $k = 0.28$, $\delta = 0.99$, and $\alpha = 0.56$. In terms of t the optical depth of a transition with wavelength λ is

$$\tau = \frac{\pi e^2}{m_e c} gf\lambda \frac{(n_l/g_l) - (n_u/g_u)}{\rho \sigma_e v_{\rm th}} t . \quad (3)$$

Quasars have much harder spectra than O stars, so that for a given value of t, the gas in a quasar wind will be in a higher ionization state than the gas in an O-star wind. The higher ionization quasar wind will not scatter the incident flux as efficiently as an O-star wind with the same t, so the force multiplier will be smaller in the quasar wind. In § 3.1, we present line force calculations using a spectral energy distribution appropriate for radio-quiet quasars. There we find $k = 1–2 \times 10^{-3}$ and $\alpha = 0.8–0.9$ for velocities below about 10,000–20,000 km s^{-1}, depending on the value of U at the face of the wind. Above this velocity the ionization state of the wind changes abruptly, and the value of k drops by a factor of about 3, while α remains unchanged. The wind velocity is primarily radial for $z \gtrsim z_0$. In this limit the fluid equations in spherical coordinates are

$$v_r \frac{\partial v_r}{\partial r} = -\frac{GM}{r^2}\left[(1-\tilde{\Gamma})\left(1-\frac{r_f}{r}\right) - \tilde{\Gamma}\left(\frac{N_{11}}{W_r}\right)^{\delta} k\left(\frac{\partial v_r/\partial r}{\sigma_e v_{\rm th}\rho}\right)^{\alpha}\right] - \frac{1}{\rho}\frac{\partial P_g}{\partial r} , \quad (4)$$

$$v_r \frac{\partial v_\theta}{\partial r} = \frac{GM}{r^2}\left[\frac{r_f(1-\tilde{\Gamma})}{r}\cot\theta - \frac{z_0}{r} - \frac{z_0}{r}\xi\left(\frac{N_{11}}{W_\theta}\right)^{\delta} k\left(\frac{\partial v_r/\partial r}{\sigma_e v_{\rm th}\rho}\right)^{\alpha}\right] - \frac{1}{\rho r}\frac{\partial P_g}{\partial \theta} . \quad (5)$$

We have taken the specific angular momentum $rv_\phi \sin\theta \approx rv_\phi = $ const. and assumed that the streamline originates at radius r_f. We neglect terms involving derivatives of the form $\partial/\partial\theta$ in all the radiation terms because the radial gradients are larger whenever radiation forces are important. The line force in the radial direction is due to UV photons emitted from the central regions, while the line force in the θ direction is due to UV photons emitted by the disk directly below the wind. The disk UV photons constitute a fraction $\xi(r) \equiv F_{\rm UV}/F$ of the total flux from the regions directly below the wind. The disk dilution factor $W_\theta \approx \frac{1}{2}$ in contrast to the dilution factor for radiation from the central source $W_r \approx (\frac{1}{4})(10^{15}\ {\rm cm}/r)^2$.

In a line-driven wind the sonic point occurs at a vertical optical depth τ of order 0.1 because the line driving is unimportant for larger optical depths. The vertical optical depth at the sonic point is similar to that in a static disk atmosphere at the same height, since in both cases hydrostatic equilibrium is a moderately good approximation (the line driving is not yet the dominant term). As a result, the disk atmosphere, which has a scale height of order z_0 (Shakura & Sunyaev 1973), obscures the line of sight from the sonic point (and from the critical point, which is very close to the sonic point) to the central source. We model this obscuration by an optical depth of the form $\tau = \tau_0 \exp[-(z - z_0)/z_0]$, in effect replacing Γ in the radiation pressure terms by $\tilde{\Gamma} \equiv \Gamma \exp(-\tau)$[4]. The vertical optical depth ≈ 0.1 at $z = z_s$ or $z = z_c$, but sight lines to the central source pass through 10–50 times more material (depending on the height of the central source), so we take the optical depth to the central source to be $\tau_0 \approx 1–5$.

Assuming a wind mass-loss rate $\dot{M}_w$ and using the relations $\rho = \dot{M}_w/(4\pi r^2 v_r)$ and $P_g = \rho a^2$ in equation (2), we find

$$\left(1 - \frac{a^2}{v_r^2}\right) r^2 v_r \frac{\partial v_r}{\partial r} = -GM\left\{(1-\tilde{\Gamma})\left[1 - \frac{r_f}{r}\right]\right\} + 2a^2 r - r^2 \frac{da^2}{dr} + \frac{(N_{11}/w_r)^{\delta}\tilde{\Gamma} GMk}{(\sigma_e v_{\rm th}\dot{M}_w/4\pi)^{\alpha}}\left(r^2 v_r \frac{\partial v_r}{\partial r}\right)^{\alpha} . \quad (6)$$

This equation is similar to the one used by CAK to describe O-star winds. It can have zero, one, or two solutions, depending on the values of the various parameters and the value of r. A steady wind is described by the unique solution that starts at low velocity, passes through a sonic point at r_s, then through a critical point at r_c, and thence out to infinity at a finite velocity. One can find the velocity, acceleration, mass-loss rate, and radius at the critical point using a simple modification of the calculation in CAK. We obtain an approximate solution to equation (6) by ignoring the inertial term and terms involving a,

$$v = v_\infty\left(1 - \frac{r_f}{r}\right)^{\beta} , \quad (7)$$

with $\beta = (1 + \alpha)/(2\alpha - \delta)$. Ignoring the inertial term corresponds to the physical statement that the line acceleration is set by the effective gravity. Using this expression, we find $r_c - r_f \approx (1 - \alpha + \delta\beta) r_f/\tau_0$, and

$$v_\infty \approx \sqrt{\left(\frac{\tau_0}{1 - \alpha + \delta\beta}\right)^{(1+\alpha+\delta)/(2\alpha-\delta)} \frac{\alpha(2\alpha - \delta)}{1 - \alpha^2} \frac{GM(1 - \tilde{\Gamma}_c)}{r_f}} , \quad (8)$$

where $\tilde{\Gamma}_c \approx \Gamma \exp\{-[\tau_0 - (1 - \alpha)]\}$. Since $(z_c - z_0)/z_0 \approx (1/10)(r_c - r_f)/r_f$, the critical point is just above the surface of the disk.

Numerical integrations show that the form (7) is a good description, while the terminal velocity is an overestimate.

The length scale of the flow is $l = v/(dv/dr)$. For velocities above the sound speed equation (7) implies $l \approx r - r_f$, the distance from the footpoint. Below the sound speed the second term on the left-hand side and the first term on the right-hand side of equation (6) are the dominant terms. Equating them and solving, we find $l \approx r(a/v_\phi)^2[r/(r - r_f)]$. Adding the two estimates gives a good approximation to the length scale of the flow at all velocities, as illustrated by Figure 2. The minimum length scale is $l = 2(a/v_\phi)r_f \approx 2 \times 10^{-3} r_f$, or 2×10^{13} cm. We note that this is less than the scale height z_0 of the disk for $\Gamma = 0.5$.

The mass-loss rate can be expressed exactly, but the equation is unwieldy. If we neglect terms of order $a/v_\phi(r_f)$, an

[4] We note that $\tilde{\Gamma} \ll 1$ at all r for which the centrifugal terms are significant. This enables us to write $1 - \tilde{\Gamma}(r_f) \approx 1 - \tilde{\Gamma}$ in the centrifugal terms to simplify the analysis.

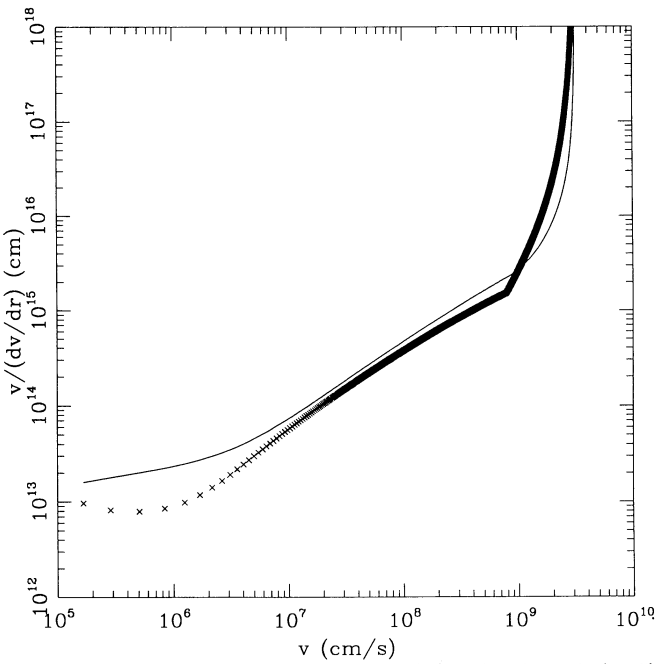

FIG. 2.—Length scale $l \equiv v/(dv/dr)$ in the wind plotted against velocity. The points are from numerical integrations of the radial component of the momentum equation, while the solid line is the approximation $l \approx (r - r_f) + r(a/v_\phi)^2[r/(r - r_f)]$ described in the text immediately following eq. (8). The break in the numerical results at $\sim 10^9$ cm s^{-1} is due to the abrupt change in the force law at that velocity. The mass of the central hole is $10^8 M_\odot$, $\Gamma = 0.5$, and $r_f = 9 \times 10^{15}$ cm.

approximate expression is

$$\dot{M}_w \approx \alpha \frac{4\pi GM}{\sigma_e v_{\rm th}} (\tilde{\Gamma}_c\, k)^{1/\alpha} \left[\frac{\tau_0}{(1 - \tilde{\Gamma}_c)}\right]^{(1-\alpha)/\alpha} . \quad (9)$$

This is the mass-loss rate into 4π sr. The actual mass-loss rate is $f\dot{M}_w$, where f is the wind cover fraction. In our models we typically find a wind mass-loss rate that is less than 10% of the mass accretion rate. Past the sonic point, the line force is of order the effective gravity (gravity plus the radial component of the centrifugal force) but oppositely directed, as we noted above. The wind efficiency, defined as $\dot{M}_w v_\infty/(L/c)$, is of order unity for $\tau_0 \gtrsim 1.0$ and decreases with increasing τ_0.

An approximate solution to equation (5) along a streamline can be found as follows. The first term on the right-hand side must balance the second when the optical depth is large (this sets the height of the disk). Neither of these terms varies rapidly as the flow moves up through the first scale height above the disk. We conclude that the third term on the right-hand side (the line-driving term) sets the scale of the acceleration. Examination of equations (4) and (5) shows that the line acceleration in the vertical direction is

$$g_{\rm line} \approx \frac{GM}{r^2} \frac{z_0}{r} \xi \left(\frac{1 - \tilde{\Gamma}}{\tilde{\Gamma}}\right)\left(1 + \frac{r_f}{r}\right), \quad (10)$$

where we neglect the left-hand side of equation (4). Integrating we find

$$v_\theta \approx -v_r(z_0/r_f)\xi(1 - \tilde{\Gamma})/\tilde{\Gamma} \quad (11)$$

for $\Delta r = (r - r_f) < r_f$. That is, the ratio $v_\theta/v_r \approx (z_0/r_f)\xi(1 - \tilde{\Gamma})/\tilde{\Gamma}$ is approximately constant, while the line driving is substantial. For $\Delta r \gtrsim r_f$ the line acceleration drops as $1/r^3$ and v_θ is essentially constant. The corresponding $\Delta\theta \approx (z_0/r_f)\xi(1 - \tilde{\Gamma})/\tilde{\Gamma} \ln(r/r_f)$ agrees well with numerical integrations of the two equations of motion. Near the inner edge of the wind, the opening angle of a streamline can change by $\xi(1 - \tilde{\Gamma})/\tilde{\Gamma} \ln(r/r_f)$ or 20%–50%.

Figure 1 illustrates the geometry of the wind. In order for the gas on the innermost streamline to flow out to large radii, it must be accelerated beyond the critical point. As the gas accelerates, its density declines, and U rises. When U exceeds a critical value $U_{\rm max}$, the soft X-rays in an unshielded active galactic nucleus (AGNs) spectrum strip too many electrons from the relevant elements, eliminating the resonance-line radiation pressure. Our photoionization calculations show that $U_{\rm max} \approx 60$ for conditions relevant to a disk wind. If the wind is exposed to the soft X-rays from the central source, its ionization state at the critical point will be so high that no line driving will occur. However, gas flow along the innermost wind streamline produces pressure gradients that accelerate neighboring gas. Gas interior to the wind thus "hitchhikes" above the disk and can shield the wind from soft X-rays. The lightly stippled area in Figure 1 indicates the position of the hitchhiking gas. The somewhat indistinct boundary between the hitchhiking gas and the wind occurs where X-ray shielding is sufficient to allow resonance-line acceleration past the critical point.

Hitchhiking gas that leaves the disk at radius r_f has an ionization parameter $U(z; r_f)$ at radius r and height z. At small z, corresponding to low velocity and high density, $U(z; r_f) < U_{\rm max}$, and the gas is pushed by resonance-line pressure. Since there is little gas above the hitchhiking gas, it feels a pressure gradient force in the $-\hat{e}_\theta$ direction, represented by the last term in equation (4). The hitchhiking gas thus accelerates upward away from the inner edge of the wind. Because the ionization parameter of the hitchhiking gas increases with velocity, line driving ceases at some height $z_{\rm max}$ where $U(z_{\rm max}; r_f)$ exceeds $U_{\rm max}$. Suppose that the critical point on the innermost streamline is at a height z_c. If the maximum height of the hitchhiking gas $z_{\rm max}$ exceeds z_c, the hitchhiking will shield the wind. Increasing the initial radius r_f will decrease $U(z; r_f)$ at any height, so for large enough initial r_f, the hitchhiking gas will shield the wind. We call the smallest such initial radius r_U, the radius of the inner edge of the wind. The ionization parameter of the gas on the innermost streamline is much larger than $U_{\rm max}$, but the absence of soft X-rays (demonstrated below) allows the gas to remain in an ionization state low enough to absorb UV photons. In O stars, which have very small X-ray fluxes, line driving occurs at values of U exceeding 1000.

To find r_U we have integrated equations (4) and (5) numerically, starting at z_0 with $v_r \sim 10^4$ cm s^{-1} and a specified r_f. The estimated critical radius $r_c \approx r_f[1 - (1 - \alpha)/\tau_0]$ allows us to find an initial $\dot{M}_w$. We then adjust r_c until the flow passes through the critical point. We use a discontinuous power law to describe the driving: $\alpha = 0.9$ at all velocities, while $k = 2 \times 10^{-3}$ for $\lesssim 10{,}000$ km s^{-1}, dropping to $k = 5.2 \times 10^4$ at higher velocities, for reasons explained in § 3.1. Having found a streamline, we then integrate equation (5) to see if the ionization parameter of the hitchhiking gas $U(z_c, r_f) < U_{\rm max}$. If it is, we start over with a smaller r_f; if it is not, we increase r_f. A few iterations yield r_U. Figure 3 shows the velocity as a function of distance along the innermost streamline. The dashed line illustrates the estimate obtained by using equation (8) in equation (7). Figure 4 shows the number density along that streamline as a function of velocity. The analytic estimates for the mass-loss rate, $\dot{M}_w \approx 10^{26} f$ g s^{-1}, and critical radius are

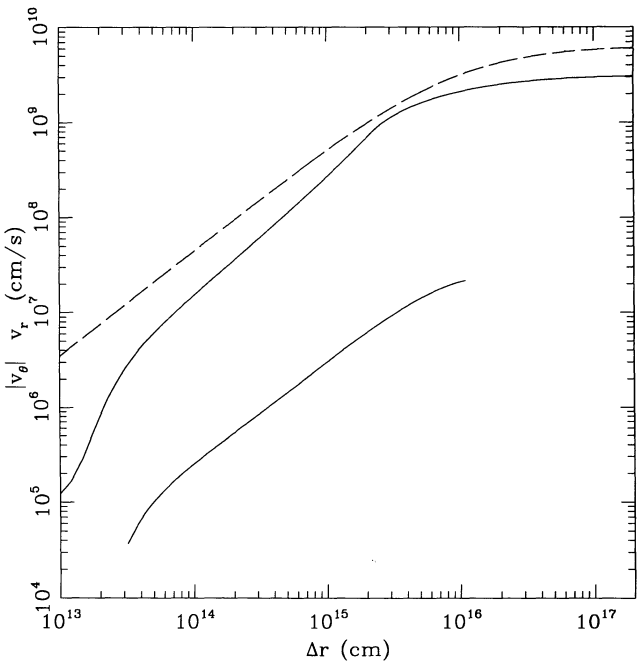

FIG. 3.—Velocities v_r and $|v_\theta|$ along the innermost streamline as a function of distance along the streamline. The dashed line shows the radial velocity predicted by eqs. (7) and (8). Parameters are as in Fig. 2.

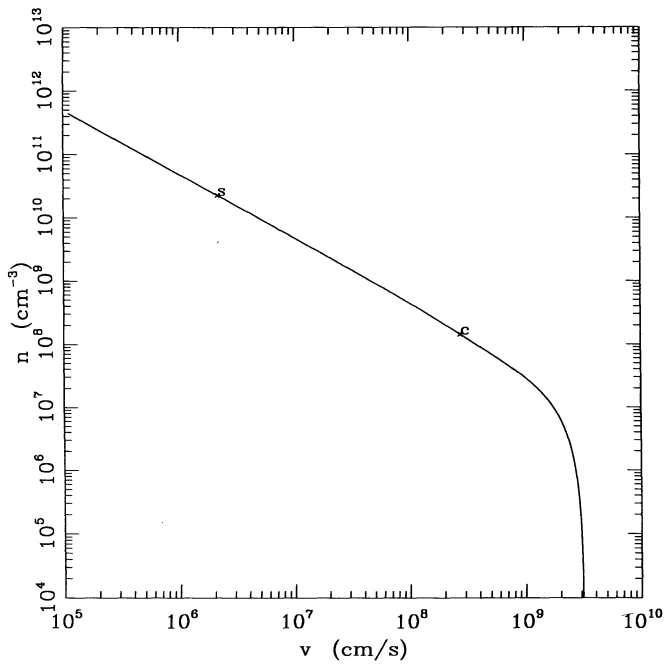

FIG. 4.—Density along the innermost streamline as a function of velocity. The sonic and critical points are marked by s and c. Parameters are as in Fig. 2.

within 20% of the corresponding numerically determined quantities. The covering fraction $f \approx 0.04$ for $\Gamma = 0.5$ and $f \approx 0.1$ for $\Gamma = 0.9$. The radius of the innermost streamline is $r_U = 9 \times 10^{15}$ cm for $\Gamma = 0.5$ and 8×10^{15} cm for $\Gamma = 0.9$.

What happens to the hitchhiking gas after it becomes highly ionized? After the line driving ceases to be important, the gas follows a Keplerian orbit and falls back to the disk at a radius smaller than that at which it started. The gas starts out on a circular small inclination orbit with a semimajor axis $a_U = r_U$. After it is accelerated by the line driving, it is on an eccentric, inclined orbit with a somewhat larger semimajor axis; $\delta a/a_U \approx v_{\rm max}/v_\phi \approx 10^{-2}$. Here $v_{\rm max}$ is the velocity at which the line driving ceases to push the gas. Typically we find $v_{\rm max} \approx 10^7$ cm s^{-1}. If the specific angular momentum is constant the product $a(1 - e^2) = \text{const}$, and $e = (\delta a/a_U)^{1/2}$. The periapsis of the hitchhiking gas is $a(1 - e) \approx a_U(1 - e)$ to lowest order in

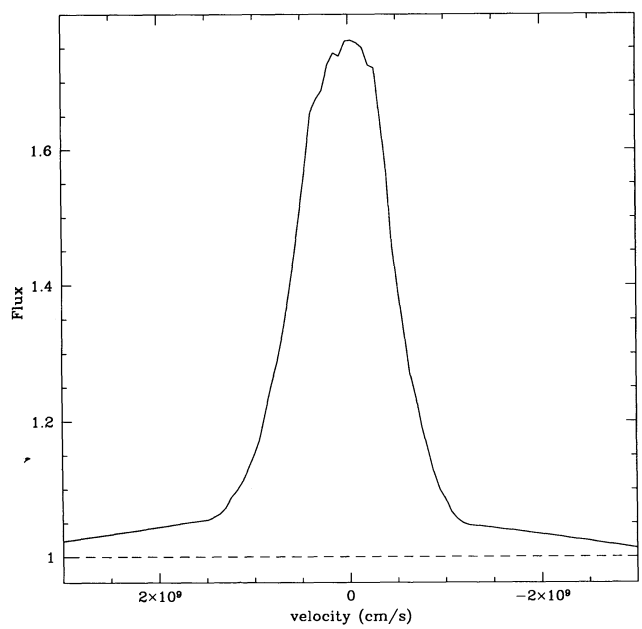

FIG. 5a

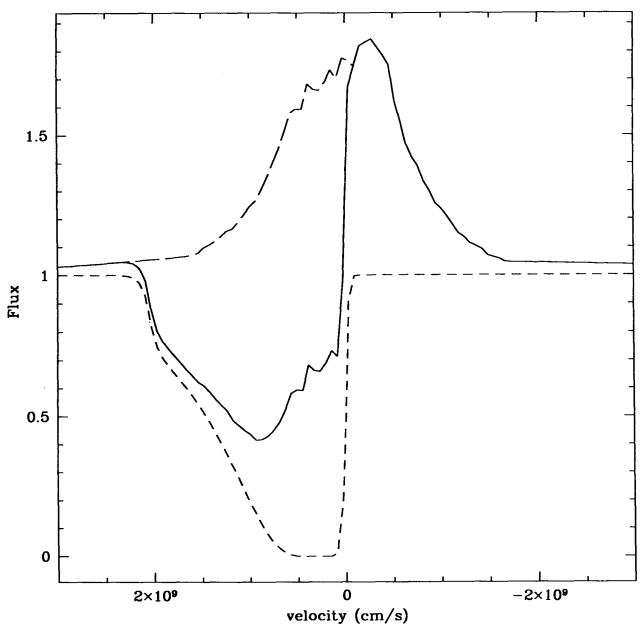

FIG. 5b

FIG. 5.—Line profiles for the C IV 1550 Å line from a disk wind seen at an inclination of (*a*) 50° (outside the wind) and (*b*) 85° (through the wind). The calculation is described in the text.

$(\delta a/a_U)^{1/2}$. The periapsis is near the line of nodes, so for $a_U = r_U = 10^{16}$ cm, the hitchhiking gas falls 10^{15} cm inside the inner edge of the wind.

When the disk is viewed nearly edge-on, the wind will be seen in absorption, and the object will be classified as a BAL QSO. Figure 5*b* shows the profile of a resonance line from an edge-on disk wind. Since the disk is rotationally supported, the effective gravity near a footpoint is small, and the wind accelerates more slowly than in the CAK solution. As a result, these absorption profiles differ qualitatively from those seen in O stars. The dimensionless optical depth along a streamline is, from equation (1), $t \sim 1/(r^2 v\, dv/dr) \sim 1/v^{(2+\delta)/(1+\alpha)}$, compared to the CAK result $t \sim$ const. Thus the disk wind model predicts BAL profiles that are deepest near line center, with the depth of absorption decreasing as the velocity increases. This purely dynamical decrease in the optical depth with increasing velocity is enhanced by the decreasing ionization fraction of such commonly observed ion as C IV. The overall result is a distinct decrease in the depth of absorption with increasing velocity. Observed BAL spectra do show this behavior, whereas O-star absorption lines have absorption maxima near the high-velocity end of the line profile.

Our calculated cover fractions indicate that 10% of all quasars should be BALQSOs, close to the observed rate. Because the wind streamlines are not radial, being more vertical at low ($\lesssim 5 \times 10^8$ cm s^{-1}) velocity, lines of sight that graze the upper edge of the wind intercept gas that is already substantially accelerated, thus missing the low-velocity portion of the wind. Disks viewed at angles near the opening angle λ should therefore have absorption troughs that start several thousand kilometers per second blueward of the systematic velocity. In our numerical integrations, the change in opening angle $\Delta\lambda$ exceeds 20%, consistent with the frequency of "detached troughs" in BALQSOs (Turnshek 1987).

3. SHIELDING AND IONIZATION

Shielding is crucial to the acceleration of the wind and determines the irradiating spectrum that the broad-line gas actually sees. Here we demonstrate that shielding can indeed permit acceleration to high velocities. We present analytical and numerical calculations of the ionization structure in the wind. The column density along the line of sight through the wind is determined by the angle between this line and the disk. Because the wind (and the hitchhiking gas) accelerates rapidly, the column accumulates near the point at which the line of sight to the central source meets the inner edge of the flow. The scale length of the flow at low velocity is of order 10^{13}–10^{14} cm and its density is of order 10^{10} cm^{-3}, so the column will be in the range 10^{23}–10^{24} cm^{-2}. Our picture of the hitchhiking gas is sufficient to produce the shielding but is not necessary. It may be that there is some other mechanism for shielding the wind, such as a Compton-heated atmosphere just interior to the wind. The main point is that some form of shielding is necessary if radiatively accelerated gas is to reach the observed velocities.

The ionization structure of the hitchhiking gas can be outlined analytically. In a gas of solar abundances, H, He, C, N, and O absorb most of the soft X-rays, if they are not fully stripped of their electrons. For simplicity, we approximate the quasar spectrum by a power law, $F_\nu \propto \nu^{-\beta}$, from the hydrogen edge through the soft X-ray band. On the inner face of the shielding gas, the CNO elements are either fully ionized or hydrogenic. Hydrogenic ions of atomic number Z have ionization energies and recombination coefficients that scale as Z^2 and ionization cross sections that scale as Z^{-2}. At the exposed face of the hitchhiking gas, the ratio of hydrogenic to fully stripped ions of element Z is thus $1.4 \times 10^{-6}\, Z^{2\beta+4} U^{-1}$. For $U = 60$ and $\beta < 2.0$, ions up to oxygen are fully ionized, while for $\beta < 1.6$, Ne is stripped as well. An element Z of numerical abundance X_Z relative to hydrogen goes from fully stripped to predominantly hydrogenic at $N_{\rm H}(Z) = 10^{23} U Z^{-2\beta-2} X_Z^{-1}$ cm^{-2}. For $\beta > 1$ and the abundances of Morton (1991), the oxygen and helium Strömgren layers are thinner than the ionized hydrogen layer. When $\beta > 1.4$, the C, N, and Ne layers are also thinner than the ionized hydrogen layer. Hitchhiking gas can therefore be optically thick to soft X-rays (above the He II edge) but transparent to UV photons.

We have computed photoionization models of the wind using the code CLOUDY (Ferland 1993). We allow model AGN spectra to irradiate the wind, normalizing the flux to obtain $1 < U < 60$ at the exposed face. This range in U corresponds roughly to the range in density at the face of the wind. Photons entering near the upper edge of the wind see lower density gas, while photons entering the wind nearly parallel to and near the surface of the disk encounter denser gas. The run of density along a radial vector differs from the run along a wind streamline because of the curvature of the streamlines. Using equations (7) and (11) we can find the base of the streamline passing through any point in the wind and hence the density at that point. Because streamlines are convex, the density falls less rapidly along radial lines that it does along a streamline.

In choosing the model spectra, it is important to note the differences between radio-loud and radio-quiet quasars. Radio-loud quasars are more luminous (Tananbaum et al. 1986; Worral et al. 1987) relative to the optical and harder in the X-ray band than radio quiet quasars (Wilkes & Elvis 1987; Williams et al. 1992). The X-ray luminosity is characterized by the nominal energy index connecting the optical to the X-ray band, defined as

$$\alpha_{\rm ox} \equiv -\log \frac{L_{(2\ {\rm keV})}}{L_{(2500\ {\rm \AA})}} \Big/ \log \frac{\nu_{(2\ {\rm keV})}}{\nu_{(2500\ {\rm \AA})}} . \qquad (12)$$

To model radio-loud quasars, we use the Mathews & Ferland (1987) spectrum, in which the drop in luminosity from the optical to the X-ray band is characterized by $\alpha_{\rm ox} = 1.4$, and a power-law slope of -0.7 above 0.4 keV. To model radio-quiet quasars we use the Mathews-Ferland spectrum with a modified X-ray band, namely (Boyle 1993; Sanders et al. 1989) $\alpha_{\rm ox} = 1.5$ and a power-law slope of -1 for both soft (Wilkes & Elvis 1987) and hard (Williams et al. 1992) X-rays. Radio quiet quasars show a range in $\alpha_{\rm ox}$ from 1.1 to 1.9.

Figure 6 plots the transmitted (radio-quiet) spectrum for three different column densities, $N_{\rm H} = 10^{22}$, $N_{\rm H} = 10^{22.5}$, and 10^{23} cm^{-2}, with $U = 10$. If the disk wind model is correct, the X-ray fluxes observed from BALQSOs should be suppressed relative to those from non-BALQSOs. The column to the central source will be of order 10^{23} cm^{-2}, and the quasar will be nearly black in soft X-rays. We note that the gas is optically thin at the Lyman edge because the ionization parameter is so large.

Figure 7 shows how the optical depths of the observed BAL lines vary with velocity, assuming $U = 10$ where the line of sight passes through the inner edge of the wind increasing to

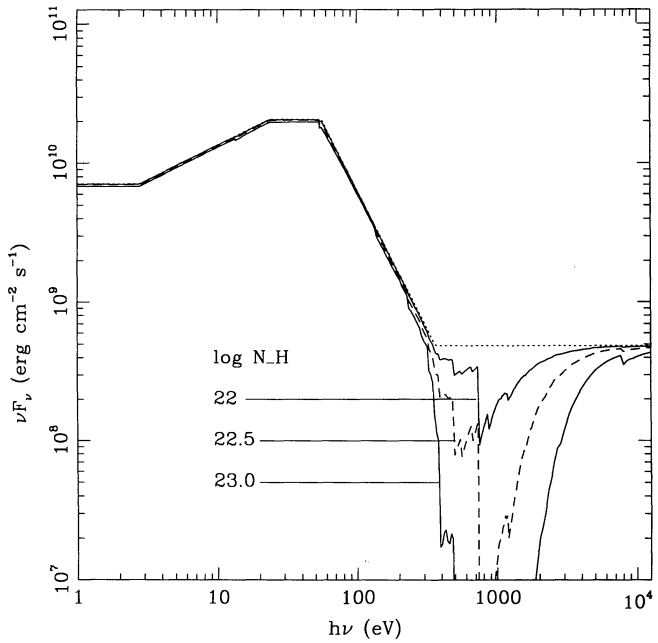

FIG. 6.—Transmitted spectrum emerging from a solar abundance wind with three different column densities but with $U = 10$ at the face of the wind. The incident spectrum is a modified Mathews-Ferland AGN spectrum, as described in the text.

$U = 2 \times 10^5$ at v_∞. The usual absorption features (O VI, N V, C IV, Si IV, and Lyα) imply minimum column densities (Weymann, Turnshek, & Christiansen 1985) $N_{O+5} > 10^{16.3}$ cm^{-2}, $N_{N+4} > 10^{16.4}$ cm^{-2}, $N_{C+3} > 10^{16.2}$ cm^{-2}, $N_{Si+3} > 10^{15.4}$ cm^{-2}, and $N_{H0} > 10^{15.5}$ cm^{-2}. In the wind model the column densities of the ions responsible for these lines exceed these lower limits, sometimes by several orders of magnitude. Lines like N V and C IV are highly optically thick at low velocity but optically thin at high velocity. C IV passes through optical depth unity at $v \approx 5000$ km s^{-1} on a line of sight with a column density of 10^{23}. We show below that, while the C IV line is optically thick when the radial velocity is small, the trough is not black near line center. Gas at low radial velocity (high density) produces a substantial amount of collisionally excited emission. This emission fills in the absorption trough at the smallest blueshifts. As a result, objects with strong, broad emission lines should have shallower absorption at low velocity than objects with narrower or weaker emission lines.

Since harder X-rays penetrate the shielding gas, they can potentially ionize away the ions (such as Ne VIII) that drive the wind, particularly at higher velocities at which densities decline dramatically. In that case the force multiplier $M(t)$ can decline dramatically as the density drops below some critical value. If this happens, then the acceleration might stop before high velocities are reached, and v_∞ is only an upper limit to the wind terminal velocity.

To estimate the maximum attainable velocity, we first note that $\dot{M}_w v_{max} \leq L/c$. Using the relation

$$U = \frac{\int_{\nu_0}^{\infty} (L\nu/h\nu)d\nu}{4\pi r^2 nc} = \frac{L/\langle h\nu \rangle}{4\pi r^2 nc}, \quad (13)$$

we find $v_{max}(U) \approx 25{,}000(U/100{,}000)^{1/2}$ km s^{-1}, where we assume that the average energy $\langle h\nu \rangle$ of an ionizing photon is 5 ryd. Next, we estimate the maximum value of U for which the wind is in the "low" ionization state. This is much larger than U_{max} at the face of the wind because the soft X-ray flux is negligible. We assume that C IV is a good tracer of the ions that drive the wind; note that the C V ion has no resonance lines in the UV. The C IV photoionization cross section at 3 keV is (Reilman & Manson 1979) $\sigma_{C\,IV} = 2 \times 10^{21}$ cm^2, while the recombination coefficient of C V is (Shull & Van Steenberg

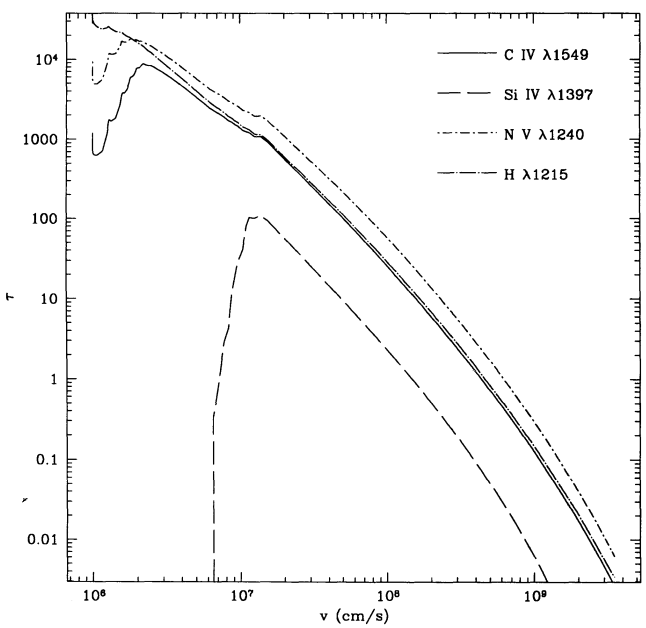

FIG. 7a

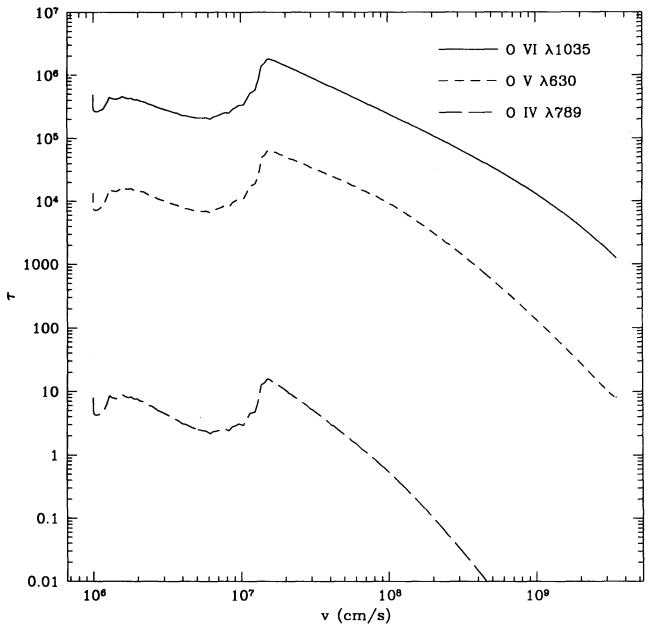

FIG. 7b

FIG. 7.—Line optical depth in the wind along a line of sight with $U = 10$ at the face of the wind irradiated by the unshielded continuum in Fig. 5. (*a*) Optical depth in C IV (*solid line*), Si IV (*long-dashed line*), N V (*dot–short-dashed line*), and Lyman-α (*dot–long-dashed line*). All these lines are optically very thick below 1000 km s^{-1} but become optically thin at higher velocities. (*b*) Optical depth in oxygen lines: O VI (*long-dashed line*), O V (*short-dashed line*), and O IV (*solid line*). There is no O III along this line of sight.

1982) 7.5×10^{-12} cm^3 s^{-1}. Hence the ratio of C IV to C V is $221^{\beta}/(8U)$ when shielding gas blocks photons between 54 eV and 3 keV and transmits all harder radiation. Choosing a limiting ratio of 10^{-2} so that the optical depth of the C IV line is unity, we find $U = 12.5 \times 221^{\beta}$, or $4 \times 10^4 \lesssim U \lesssim 6 \times 10^5$ for $1.5 < \beta < 2$. Hence 16,000 $\lesssim v_{\max} \lesssim$ 60,000 km s^{-1}. As the gas accelerates from a velocity of 10 km s^{-1} to 25,000 km s^{-1}, the ionization parameter increases from 40 to 100,000.

3.1. *A Self-consistent Force Law*

To obtain a more complete and accurate picture of the effect of X-rays on the wind, we use CLOUDY in combination with the dynamics to redo Abbott's O-star force law calculation for a quasar spectrum. In this way we can find a self-consistent wind solution, in which the force law obtained by adding up the contributions from all the ions in the wind is the same as the force law used in the dynamical calculation of the wind velocity and density. Using CLOUDY allows us to account for the attenuation of X-rays into the wind.

We employ an iterative procedure. First, we assume a force law of the form given by Abbott (1982). Using this force law we calculate the density and velocity in the wind as described above. We then use CLOUDY to calculate the ionization state of the 16 most abundant elements, using solar abundances and illuminating the face of the wind with our modified Mathews-Ferland spectrum. Assuming that all ions are in the ground state, so that only resonance lines can scatter photons, we then add up the force for all the resonance lines in the list compiled by Verner, Barthel, & Tytler (1994). The force multiplier is

$$M(t) = \sum_{\text{lines}} \frac{\nu_l F_{\nu l}}{F} \frac{v_{\text{th}}}{c} \frac{1}{t} (1 - e^{-\tau_l}) , \qquad (14)$$

where F_ν is from the modified Mathews-Ferland spectrum and the line optical depth is given by equation (3). We fit this numerical force law to obtain the new (power law) estimate for $M(t)$. Two or three iterations suffice to converge on a self-consistent force and velocity law pair. We find $k = 1$–2×10^{-3} and $\alpha = 0.8$–0.9, depending on the line of sight (or on U at the face of the wind). The maximum value of the force multiplier in our wind is ≈ 10 with $t = 1 \times 10^{-4}$.

Figure 8 shows that tens to hundreds of lines contribute to the driving. All the commonly observed lines such as O VI and C IV contribute significantly to the driving, but at high velocity $v = 10{,}000$ km s^{-1} (small t) Mg V–X, Fe VII–XI Si VIII–XI, and Ne V–VIII are among the most important ions. At low velocity (100 km s^{-1}) lower ionization species predominate, but higher ionization states such as Ne VIII still contribute substantially. Ne VIII has a resonance line at 774 Å that is accessible to *HST* for moderate redshifts and to ground-based instruments in high-redshifts quasars. This line should be seen in emission and 10% of the time in absorption in radio-quiet quasars. Recently Hamman, Zuo, & Tytler (1995) reported finding Ne VIII emission in three moderate-redshift quasars.

Figure 9 shows the force multiplier $M(t)$ (*solid line*) and the velocity (*dashed line*) as a function of t. Along this line of sight the numerically determined line force abruptly drops at $t = 4 \times 10^{-5}$ ($v \approx 10{,}000$ km s^{-1}), and the temperature of the gas soars. This is a result of the loss of ions suitable for driving the wind and corresponds to reaching the limit found in the analytic calculation of the ratio of C IV to C V given above. We model this abrupt change in $M(t)$ by using two power laws with the same slope $\alpha = 0.9$ but with different values of k. For

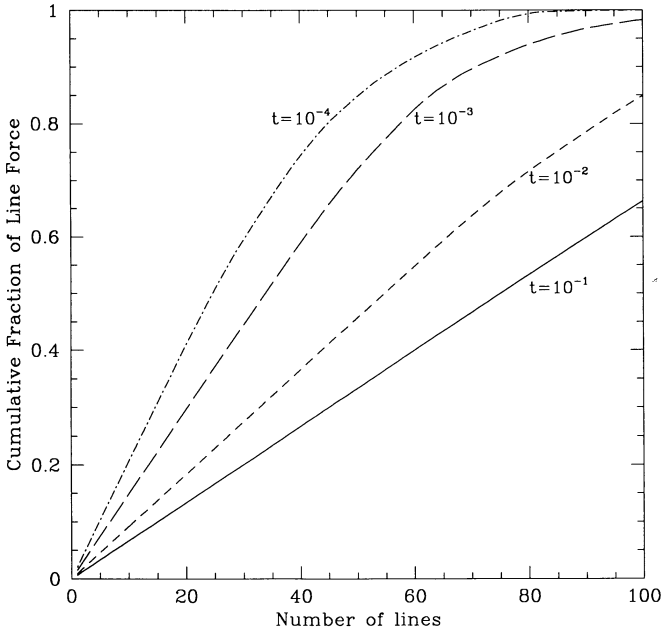

FIG. 8.—Cumulative fraction of the force multiplier $m(t)$ vs. number of lines for four different values of t.

$t > 4 \times 10^{-5}$ we find $k = 2 \times 10^{-3}$, while for $t < 4 \times 10^{-5}$ $k = 5.2 \times 10^{-4}$. With this force law, the terminal velocity is 30,000 km s^{-1}, as shown in Figure 3.

Objects with harder spectra ionize away the resonance-line absorbing species at higher densities, limiting the terminal velocities of their line-driven winds to lower values. For example, using the Mathews-Ferland spectrum, we find that the wind stops accelerating at a velocity of $\sim$3–5000 km s^{-1}. This could be why broad absorption lines have never been seen in a radio-loud quasar. Similar remarks apply to Seyfert 1

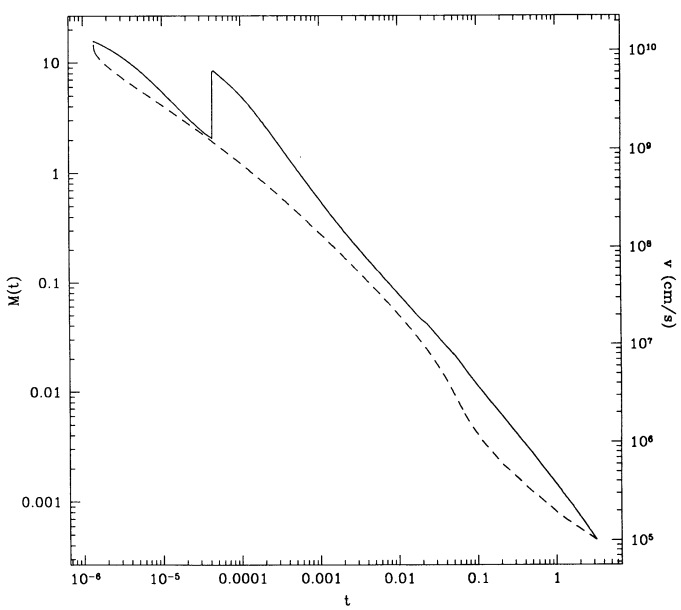

FIG. 9.—The force multiplier $M(t)$ (*solid line, left-hand scale*) and velocity v (*dashed line, right-hand scale*) as functions of the dimensionless optical depth t. The ionization parameter at the face of the wind is $U = 10$.

galaxies, which also possess harder X-ray spectra than radio-quiet quasars.

4. BROAD EMISSION LINES FROM DISK WINDS

The broad-line emitting region cannot lie outside the broad-line absorbing region. This follows from the observation that Lyman-α emission is diminished by the N v absorption trough in some BAL quasars (Turnshek 1987). The emission could be cospatial with the absorption. In an outwardly accelerating flow, all points are redshifted with respect to one another. Encircling each point in a flow that emits Lyα is a surface where these Lyα photons have redshifted into the N v line and can be absorbed. Thus Lyα emission can come from the same flow that produces N v absorption. Turnshek (1987) has pointed out the apparent existence of a correlation between the morphology of the emission and absorption troughs in BALQSOs. Such a correlation would suggest that the emitting and absorbing flows are physically connected.

A consideration of the energetics of the wind suggests that much of the observed line emission could come from the wind. This statement depends on the flux of ionizing radiation, particularly in the extreme UV region of the spectrum which is difficult to observe. Marshall et al. (1995) used the *EUVE* satellite to observe the Seyfert I galaxy Mrk 478. They find a very large soft X-ray/extreme UV excess, much larger than that in the Mathews-Ferland spectrum. However, let us take the UV flux in the Mathews-Ferland spectrum as a lower limit. The emission spectrum, Mathews and Ferland use the observed power law $L_\nu = L(\nu_0\,\nu)^{-1/2}$; in their model L is roughly the bolometric luminosity and $\nu_0 = 5.7 \times 10^{15}$ Hz, corresponding to a wavelength of $\lambda_0 = 526$ Å. If the equivalent width of the Lyman-α line is EW_α, the luminosity in lines is

$$L_{\rm lines} = \int_{\nu_\alpha(1-\mathrm{EW}_\alpha/2\lambda_\alpha)}^{\nu_\alpha(1+\mathrm{EW}_\alpha/2\lambda_\alpha)} L_\nu\, d\nu \approx \frac{1}{4} L \sqrt{\frac{\lambda_0}{\lambda_\alpha}} \frac{\mathrm{EW}_\alpha}{\lambda_\alpha} . \quad (15)$$

For a typical quasar $\mathrm{EW}_\alpha \approx 100$Å, so the gas in the wind need capture only 1% of the total luminosity to power the Lyman-α emission, and $\lesssim 10\%$ to power all the lines. If Mrk 478 proves typical of AGNs, then the fraction of the luminosity captured by the wind can be even smaller.

We begin by giving an analytic estimate of the equivalent width of C IV emission from the wind. If the emission is primarily collisionally excited, it must come from the high-density low-velocity region of the wind near the surface of the disk. Our strategy is to calculate the emission from surfaces of constant radial velocity, ignoring the rotational velocity, and then integrate over v. In the numerical results presented later in this section, we calculate line profiles by taking into account the rotational motion.

The base of the wind at all radii is heated by UV radiation from the central source. The height of a constant density surface in the wind, measured from the surface of the disk, is essentially independent of radius except in the shielding gas. Consider a photon emitted from the central source in a direction roughly parallel to the disk midplane. Where will it be absorbed? The shielding gas has a continuum optical depth less than unity in the UV, so the photon will pass through into the body of the wind. Because the continuum source almost certainly produces substantial emission from a height somewhat above z_0, this emission will pass through high-velocity, low-density gas before reaching low-velocity dense gas, where it will be absorbed. That is to say, even in the extreme case that the disk height z in the region of the wind is independent of radius, the base of the wind is illuminated and heated by the central source. If the disk height increases with radius, as does the Shakura-Sunyaev gas pressure supported solution beyond 3.7×10^{16} cm, even photons on radial paths from the central source will reach the base of the wind and heat it. The optical depth along such a radius is essentially infinite, since the disk is very optically thick.

Conditions at the base of the wind are different from those in the bulk of the wind. Photons that reach the base of the wind pass through the shielding gas at lower altitudes, where the gas is denser and hence has a lower ionization parameter. Thus, the gas at the base of the wind is subject to an even softer spectrum than the gas producing the absorption, and it is in a lower ionization state. In our CLOUDY runs we model the emitting gas using a lower ionization parameter, $U = 1$–10.

Because the radius of the wind is much larger than radius of the continuum-emitting region, the area of the line-emitting region is very large compared to the area emitting the continuum. It is this large area which allows the relatively low temperature wind to be seen in emission.

4.1. C IV *Equivalent Width*

To estimate analytically the C IV equivalent width, we use the escape probability method applied to a two-level atom. We refer the reader to Castor (1970) for a good introduction to the technique. Following Castor, let $\sigma \equiv [(d\ln v/d\ln r) - 1]$. Then the emission-line profile, defined as the difference between the total and continuum luminosity (per hertz) divided by the continuum luminosity, is given by

$$F_e(v) = \frac{4\pi^2}{L_\nu} \int_{r_U}^{r_{\rm max}} (1 + \sigma \sin^2 i) \times S(r)\{1 - \exp\,[-\tau(v, r, \infty)]\} 2r\, dr , \quad (16)$$

where $S(r)$ is the source function in the wind, i is the inclination of the disk, and $L_\nu \approx 10^{31}$ ergs^{-1} Hz^{-1} is the continuum luminosity per hertz of the central source. The quantity

$$\tau(v, r, \infty) = \frac{\pi e^2}{m_e c} (gf\lambda) \frac{(n_l/g_l) - (n_u/g_u)}{v/r} \cdot \frac{1}{1 + \sigma \sin^2 i} . \quad (17)$$

is the optical depth along the line of sight from a point in the wind to Earth. The logarithmic derivative of the velocity $\sigma \approx 100$, so that for all but face-on disks ($i \lesssim 1/\sigma^{1/2}$) this optical depth is roughly equal to the optical depth along a radial line given by equation (3).

Let ϵ be the ratio of true to net absorption, where (Castor 1970)

$$\epsilon = \frac{20}{T^{1/2}} n_e \lambda^3 P\left(\frac{\chi}{k_{\rm B} T}\right) . \quad (18)$$

Here $P(\chi/k_{\rm B}T)$ is of order unity for small $\chi/k_{\rm B}T$ and is near 0.2 for large values of $\chi/k_{\rm B}T$. For a two-level atom with an unsaturated optically thick line ($\epsilon\tau/\sigma < 1$, $\tau \gg 1$), the source function is given by the product of this ratio and the Planck function, divided by the escape probability β,

$$S \approx \epsilon B_\nu/\beta \approx 3\epsilon\tau B_\nu/\sigma . \quad (19)$$

If the line is saturated ($\epsilon\tau/\sigma > 1$), then $\epsilon\tau/\sigma$ is replaced by 1.

Using this expression, the line profile becomes

$$F_e(v) \approx \frac{24\pi^2}{L_\nu} \sin^2 i \int_{r_U}^{r_{\rm max}} \epsilon\tau B_\nu\, r\, dr . \quad (20)$$

At fixed velocity only ϵ is a function of r (through n), since fixing the velocity fixes both and U and therefore $B_\nu[T(U)]$. From the continuity equation $n \sim 1/r^2$ so

$$F_e(v) \approx \frac{24\pi^2}{L_\nu} \sin^2 i\, \epsilon(r_U, v)\tau(v) B_\nu r_U^2 \ln\left(\frac{r_{\max}}{r_U}\right). \quad (21)$$

To find the equivalent width of the line, we must integrate over velocity. At low velocities the line is saturated. The density at the sound speed is $\sim 3 \times 10^{10}$ cm^{-3}. Using equation (18), $\epsilon \approx 3 \times 10^{-6}$ for the resonance line of C IV, while the optical depth $\sim 2 \times 10^7$ since essentially all the carbon is in the form of C IV. The product $\epsilon\tau \approx 60$, while $\sigma \approx 100$, so the line is nearly saturated at the sound speed. As the velocity increases, both ϵ and τ decrease. The lower limit on the velocity integral is set by the requirement that the continuum optical depth to the central source be no greater than 1, which corresponds roughly to the sound speed. Doing the integral,

$$\mathrm{EW} = \lambda \frac{24\pi^2 r_U^2 B_\nu}{L_\nu} \sin^2 i \left(\frac{\epsilon\tau a}{c}\right) \ln\left(\frac{r_{\max}}{r_U}\right), \quad (22)$$

where the equivalent width and the wavelength ($\lambda = 1550$ for C IV) are measured in angstroms. Our photoionization calculations indicate a temperature of 20,000 K for the gas, so $B_\nu \approx 10^{-3}$ ergs s^{-1} cm^{-2} Hz^{-1} s^{-1}. Assuming that the inner edge of the wind is at $r_U = 10^{16}$ cm while the outer edge is a factor 10 out, we find an equivalent width for the C IV emission line of $\sim 30 \sin^2 i$ Å.

4.2. *Numerical Line Profiles*

Our numerical calculations show that the wind produces broad emission lines because of collisionally excited emission, with a small ($\sim$20%) contribution from resonance scattering. Examples are shown in Figure 5, which shows the C IV line from a disk viewed at two different angles. As shown above, the collisional emission comes from dense gas in the base of the wind near the disk. The radial velocity of this gas is comparable to or smaller than its rotational velocity—the width of the emission line is due to the fact that the flow originates in a roughly Keplerian disk.

We use the ionization fractions from CLOUDY along with the corresponding run of velocity and density for a self-consistent wind solution as input to the line profile calculation. We use a low-U ($=2$), high initial density 3×10^{10} cm^{-3} model to approximate a line of sight along the disk and a high-U ($=20$), low initial density 5×10^9 cm^{-2} model to approximate a line of sight at a larger angle to the disk. We assume that the Sobolev approximation is valid, so the radiative transfer calculation for the formation of resonance lines is relatively straighforward. We have been guided by Castor's original line formation calculation for Wolf-Rayet stars (Castor 1970). We apply the refinements described by Rybicki & Hummer (1978) for flows which have nonlocal radiative coupling and also use their expressions for calculating the escape probabilities (Rybicki & Hummer 1983).

We calculate the line profiles assuming the observationally inferred covering fraction of the BAL region ($\sim$10%). The flow consists of a radial component given by the approximate analytic solution to the wind radial equation and an azimuthal component which results from the assumption of specific angular momentum conservation. We neglect the poloidal velocity in calculating surfaces of constant projected velocity. Although the radial velocity law is monotonic, the azimuthal velocity dependence means that multiple projected velocity surfaces will lie along certain observer lines of sight. This requires us to consider nonlocal coupling in the radiative transfer calculation.

In order to specify the temperature, we have run CLOUDY for our two sample streamlines, using our solution for the radial velocity to give the density as a function of depth into the wind. Using these results, we parameterize the temperature in terms of the ionization parameter and use this relation to specify the temperature for our line calculation.

As indicated by our analytical calculation, the temperature of the gas ($T \sim 2 \times 10^4$ K) inferred from the photoionization calculations means that a substantial amount of emission results from collisional excitation. If the emission were due only scattered photons, the mean equivalent widths of the observed emission lines would only be 10%–20% of the equivalent widths of the absorption troughs rather than the substantially larger widths which we obtain. For a typical viewing agle of 50° (Fig. 5*a*) the equivalent width is about $\sim$57 Å. The full width at half-maximum of the C IV emission is $\sim$10,000 km s^{-1}.

Wills et al. (1993) examine a large sample of quasars and find C IV equivalent widths which range from 2 to 76 Å, with a mean width of $\sim$30 Å and full width at half-maximum of $\sim$5,000 km s^{-1}, while Baldwin, Wampler, & Gaskell (1989) find a range of 12.0–209 and a mean of 49 Å for their PKS sample. Results for other metal resonance lies are similar. This suggests that the bulk of the emission in resonance lines is produced in the disk wind.

We note that, at first glance, this result would suggest that the wind will overproduce N V and O VI relative to the observations. However, the disk area over which N V and O VI ions exist in sufficient numbers to emit is likely to be much smaller than the area over which the C IV or Lyman-α emission is produced. More detailed wind modeling is needed to clarify this point.

5. DISCUSSION

The standard model for broad-line emission assumes that many clouds which are (3×10^{17})–(3×10^{18}) cm from the central source intercept 10% of the ionizing radiation and radiate it in emission lines. However, there are numerous well-known problems with the cloud model:

1. The origin of the cloud material is unclear (see, however, Emmering, Blandford, & Shlosman 1992).
2. Unconfined clouds dissipate on short timescales. Many confinement mechanisms have been proposed, but none has been generally accepted.
3. Since the thermal line widths of photoionized clouds are much smaller than the widths of the broad lines, the smoothness of the emission lines implies at least 10^4 emitting clouds, and the breadths of the absorption lines imply at least 10^4 absorbing clouds along each BALQSO line of sight.
4. The emitting clouds must have a radial extent of $\sim 10^{13.5}$ cm to produce the observed ionization states, but there is no physical length scale of this size. Similarly, there is no explanation for the much shorter inferred length scale (10^{21} cm$^{-2}/10^{10}$ cm$^{-3} \sim 10^{11}$ cm) of the absorption clouds.
5. There is no explanation for the covering fraction $\approx$0.1 of the line-absorbing gas in those objects showing broad absorption.

In the disk wind picture, these problems vanish:

1. The line-emitting gas emerges from the disk.
2. There are no clouds, so there is no confinement problem.
3. The wind naturally produces smooth line profiles in both absorption and emission.
4. We have shown how a length scale of $\sim 2 \times 10^{13}$ cm in the line-emitting gas is generated by radiative acceleration from a Keplerian disk. The length scale of the absorbing gas is much larger than is usually inferred, because the density of the absorbing gas is small. This is connected with the fact that the ionization parameter in the wind is so much larger than is usually assumed.
5. The covering fraction of the wind is $\sim 10\%$. This explains the fraction of quasars showing broad absorption. In addition, disk winds naturally explain some of the peculiar phenomenology of broad emission lines. Since the disk itself is optically thick, for most viewing geometries we see only the wind on one side of the disk. As a result, the high-ionization lines should be blueshifted relative to the low-ionization lines (Emmering et al. 1992). This shift has already been observed (Corbin 1990).

The innermost streamlines have the highest rotational and (terminal) radial velocities and the highest ionization states. Streamlines originating farther out are more effectively shielded from the central X-rays by the hitchhiking gas and the intervening wind but have smaller v_ϕ and v_∞. Thus, the wind model naturally explains the observation that the full width at half-maximum of the C IV λ1550 emission line is larger than that of Mg II λ2798 in radio-quiet quasars (Brotherton et al. 1994) as well as the stratification seen in reverberation mappings (Clavel et al. 1991).

Similar comments apply to absorption lines. The cover fraction of the Mg II wind is smaller than the cover fraction of the C IV wind, since Mg II forms on more distant, heavily shielded streamlines. Only in the very small number of cases in which we are looking through the Mg II wind will see absorption in both C IV and Mg II. In these cases, the onset of absorption in different lines will occur at zero relative redshift, but the widths of high-ionization absorption troughs will exceed those of low-ionization troughs. This effect has already been observed (Voit, Weymann, & Korista 1993). The C IV absorption in such objects will be deeper than in BAL quasars without Mg II absorption, since the cover factor of the low-velocity gas will be larger than in objects in which the disk is seen less edge-on.

6. PREDICTIONS

The disk wind makes a number of predictions which make it easily testable and which distinguish it from other models of the broad absorption and emission line regions.

1. The broad-line region is very small, $\sim 3 \times 10^{16}(L/10^{46})^{1/2}$ cm. The bulk of the N V line emission, which comes from the inner streamlines, occurs at $r_{\rm BELR} \sim 10^{16}$ cm. From equation (9), the density at the base of the wind scales as $L\Gamma^{(1-\alpha)/\alpha}$, so the size of the broad-line region scales as $L^{1/2}\Gamma^{(1-\alpha)/2\alpha}$. If most AGNs emit near the Eddington limit, $r_{\rm BELR} \sim L^{1/2}$, and the results from reverberation mapping of Seyfert galaxies (Korista et al. 1995) imply N V emitting region sizes $\lesssim 4 \times 10^{16}$ cm for luminous quasars. Such a small radius is consistent with the wind model but is much smaller than those derived from models of unshielded clouds of density $\sim 10^{10}$ cm^{-3}.
2. The ionization parameter of the emitting gas is larger, $U \sim 1$–60. As a result one expects Ne VIII and Mg IX resonance lines to be seen in both emission and absorption. At the same time, the shielding ensures that lower Z lithium-like ions (O VI, N V, C IV, etc.) will be present. Hamman, Zuo, & Tytler (1995) report the detection of Ne VIII emission from three moderate-redshift quasars. They infer an ionization parameter of 10.
3. The wind, together with the shielding gas, is thick to soft X-rays. This implies that BALQSOs will show strong absorption in the soft X-ray band. There is little observational evidence on this point, but we know of two recent *ROSAT* results that are relevant. Green et al. (1995) examined the properties of the Large Bright Quasar Survey quasars in the *ROSAT* All-Sky survey. They find that BALQSOs as a class are underluminous in X-rays compared with non-BALQSOs at the 2–3 σ level. Kopko, Turnshek, & Epsey (1994) found $1.9 < \alpha_{\rm OX} < 2.5$ from pointed *ROSAT* observations of five BALQSOs, indicating that these objects were much quieter in the X-ray band than non-BAL quasars.
4. Objects with large X-ray–to–optical flux ratios, such as radio-loud quasars and Seyfert I galaxies, will have winds with small terminal velocities and only moderately broad (2–5000 km s^{-1}) absorption lines. When such absorption is seen, these objects will also show signs of soft X-ray absorption.
5. The wind has an optical depth to electron scattering that is of order unity. If the wind is smooth and axisymmetric, electron scattering will produce continuum polarization parallel to the disk axis.

The accretion disk wind picture outlined here offers a promising new framework for interpreting the broad absorption and emission lines seen in quasar spectra. Shielding of the wind by hitchhiking gas at its inner edge allows radiation pressure on ultraviolet resonance lines to produce terminal velocities $\sim 0.1c$. The dynamical behavior of the wind appears consistent with the observed shapes of the absorption profiles and the covering factors inferred from BALQSO statistics.

N. M. thanks P. Goldreich and R. Weymann for suggesting the problem and T. Kallman for providing ionization calculations. This work was supported by NSERC of Canada and by the Connaught Fund of the University of Toronto.

REFERENCES

Abbott, D. C. 1982, ApJ, 259, 282
Arav, N., Li, Z., & Begelman, M. C. 1994, ApJ, 432, 62
Baldwin, J. A., Wampler, E. J., & Gaskell, C. M. 1989, ApJ, 338, 630
Blandford, R. D., Netzer, H., & Woltjer, L. 1990, Active Galactic Nuclei (Berlin: Springer)
Boyle, B. J. 1993, in The Environment and Evolution of Galaxies ed. J. M. Shull & H. A. Thronson (Dordrecht: Kluwer), 433
Brotherton, M. S., Wills, B. J., Steidel, C. C., & Sargent, W. L. W. 1994, ApJ, 423, 131
Castor, J. I. 1970, MNRAS, 149, 111
Castor, J. I., Abbott, D. C., & Klein, R. I. 1975, ApJ, 195, 157 (CAK)
Clavel, J., et al. 1991, ApJ, 366, 64
Corbin, M. R. 1990, ApJ, 357, 346
Drew, J. E., & Boksenberg, A. 1984, MNRAS, 211, 813
Emmering, R. T., Blandford, R. D., & Shlosman, I. 1992, ApJ, 385, 460
Ferland, G. J. 1993, University of Kentucky Department of Physics and Astronomy Internal Report
Green, P. J., et al. 1995, ApJ, 450, 51
Hamann, F., Korista, K. T., & Morris, S. L. 1993, ApJ, 415, 541
Hamman, F., Zuo, L., & Tytler, D. 1995, BAAS, 26, 1356
Korista, K. T., et al. 1995, ApJS, 97, 285
Kopko, M., Jr., Turnshek, D. A., & Espey, B. R. 1994, in IAU Symp. 159, Multi-Wavelength Continuum Emission of AGN, ed. T. J.-L. Courvoisier & A. Blecha (Dordrecht: Kluwer), 450

Marshall, H. L., Carone, T. E., Shull, J. M., Malkan, M. A., & Elvis, M. 1995, ApJ, submitted
Mathews, W. G., & Ferland, G. J. 1987, ApJ, 323, 456
Morton, D. C. 1991, ApJ, 77, 119
Osterbrock, D. E. 1989, Astrophysics of Gaseous Nebulae and Active Galactic Nuclei (Mill Valley: University Science Books), chap. 11
Reichert, G. A., et al. 1994, ApJ, 425, 582
Reilman, R. F., & Manson, S. T. 1979, ApJS, 40, 815
Rybicki, G. B., & Hummer, D. G. 1978, ApJ, 219, 654
———. 1983, ApJ, 274, 380
Sanders, D. B., Phinney, E. S., Neugebauer, G., Soifer, B. T., & Matthews, K. 1989, ApJ, 347, 29
Shakura, N. I., & Sunyaev, R. A. 1973, A&A, 24, 337
Shlosman, I., Vitello, P. A., & Shaviv, G. 1985, ApJ, 294, 96
Shull, J. M., & Van Steenberg, M. E. 1982, ApJS, 48, 95
Stocke, J. T., Morris, S., L., Weymann, R. J., & Foltz, C. B. 1992, ApJ, 396, 487
Tananbaum, H., Avni, Y., Green, R. F., Schmidt, M., & Zamorani, G. 1986, ApJ, 305, 57
Turnshek, D. A. 1987, in QSO Absorption Lines: Probing the Universe ed. J. C. Blades, D. Turnshek, & C. Norman (Cambridge: Cambridge Univ. Press), 17
Verner, D. A., Barthel, P. D., & Tytler, D. 1994, A&AS, 108, 287
Vitello, P. A. J., & Shlosman, I. 1988, ApJ, 327, 680
Voit, G. M., Weymann, R. J., & Korista, K. T. 1993, ApJ, 413, 95
Weymann, R. J., Morris, S. L., Foltz, C. B., & Hewett, P. C. 1991, ApJ, 373, 23
Weymann, R. J., Turnshek, D. A., & Christiansen, W. A. 1985, in Astrophysics of Active Galaxies and Quasi-Stellar Objects, ed. J. Miller (Mill Valley: University Science Books), 333
Wilkes, B. J., & Elvis, M. 1987, ApJ, 323, 243
Williams, O. R., et al. 1992, ApJ, 389, 157
Wills, B. J., Brotherton, M. S., Fang, D., Steidel, C. C., & Sargent, W. L. W. 1993, ApJ, 415, 563
Worral, D., Giommi, P., Tananbaum, H., & Zamorani, G. 1987, ApJ, 313, 596